Catalysis Science & Technology

Accepted Manuscript

ROYAL SOCIETY OF CHEMISTRY

www.rsc.org/catalysis

Catalytic dehydration of ethanol over hierarchical ZSM-5 zeolites regarding their acidic properties and type of generated porosity

Karolina A. Tarach [a,*], Justyna Tekla [a], Wacław Makowski [a], Urszula Filek [b], Kinga Mlekodaj [a], Vladimir Girman [c], Minkee Choi [d] and Kinga Góra-Marek [a*]

[a] *Faculty of Chemistry, Jagiellonian University in Kraków, Ingardena 3 St., 30-060 Kraków, Poland, phone: +48 12 663 2081, fax: +48 12 634 0515*
[b] *Jerzy Haber Institute of Catalysis and Surface Chemistry PAS, Niezapominajek 8 St., Kraków, Poland*
[c] *Pavol Jozef Šafárik University in Košice, Department of Condensed Matter Physics, Park Angelinum 9, 041 54 Košice, Slovakia*
[d] *Department of Chemical and Biomolecular Engineering, Korea Advanced Institute of Science and Technology, Daejeon 305-701, Republic of Korea*

Corresponding Author
*Karolina A. Tarach, Faculty of Chemistry, Jagiellonian University in Kraków, Ingardena 3 St., 30-060 Kraków, Poland, phone +48 (12) 663-20-81, fax. +48 (12) 634-05-15
E-mail address: karolina.tarach@gmail.com
*Kinga Góra-Marek, Faculty of Chemistry, Jagiellonian University in Kraków, Ingardena 3 St., 30-060 Kraków, Poland, phone +48 (12) 663-20-81, fax. +48 (12) 634-05-15
E-mail address: kinga.goramarek@gmail.com

Abstract

The catalytic activity in alcohols dehydration process has been studied with respect to acidity and porosity picture of novel micro/mesoporous ZSM-5. The choice of samples characterized by similar Si/Al ratio in range between 23 and 36 assured the ability to proper following the changes in catalytic performance related to concentration of acid sites, their accessibility and strength. Special attention has been paid to the porosity studies with involvement of low-temperature nitrogen sorption and quasi-equilibrated temperature programmed desorption of hydrocarbons. Thus the wide range of materials from typically microporous ZSM-5 to micro/mesoporous analogues obtained by different methods, however at many points still representing similar properties, allowed investigation of influence of porosity character on catalytic performance. Both the acidic picture and porosity properties that were significantly perturbed by various synthesis and modification strategies, found clear reflection in catalytic performance of hierarchical zeolites described as volcano curve dependence.

Keywords: hierarchical zeolites, ethanol dehydration, ZSM-5, accessibility, porosity

1 Introduction

Environmental concerns determine the research paths aimed at seeking alternative sources of fuels and chemicals being currently supplied by petroleum industry. For this reason the catalytic ethanol dehydration as a valuable source of diethyl ether (DEE), ethylene (C_2=) or higher hydrocarbons (C_{3+}) is in the field of interest for scientific community [1]. DEE is considered as industrially important ether used as a solvent in organic synthesis or as a substrate for higher C_n ethers. It is also applicable in fuel chemistry as additive for improved ignition properties [2]. Ethylene, an important petrochemical intermediate, allows for production of a number of products including polyethylene and when produced from bioethanol assures economic feasibility with higher purity [1].

The ethanol dehydration reaction occurs through either bimolecular pathway to generate diethyl ether in exothermic reaction or unimolecular mechanism to obtain ethylene in endothermic reaction [3, 4]. Generally, the production of DEE is highly selective reaction at low temperature and conversion, while at higher temperature both the conversion and selectivity to ethylene are enhanced. Currently three categories of catalyst for ethanol dehydration process are distinguished and investigated [1]: oxides [5], molecular sieves (zeolites and SAPO materials) [6, 7] and heteropolyacids [8, 9]. Among molecular sieves the ZSM-5 zeolite has been the most extensively investigated catalyst owing to significantly lowered temperature of ethylene formation. The main drawback of catalytic applicability of ZSM-5 zeolite in ethanol dehydration process is identified as fast deactivation of catalyst related to coke formation. Thus substantial effort of researchers has been paid on studies involving catalytic performance of hierarchical zeolites. These materials, besides intrinsic micropores possess also a system of mesopores diminishing diffusional limitations, e.g. poisoning of acid sites by coke formation. It has been proven that presence of mesopores influences the catalysts lifetime in ethanol dehydration [10], ethanol to hydrocarbons [11] and methanol to gasoline [12] processes. Furthermore, for ethanol dehydration Tsapatsis et al. [4] have shown that in kinetic regime the catalytic performance of Brønsted acid sites in zeolites possessing dual meso-/microporosity is dominated by the micropore system. This behaviour has been assigned to preferential adsorption of small alkane or alcohol reactant molecules inside micropores. However, numerous studies regarding catalytic performance of hierarchical zeolites in alcohols dehydration, do not correlate clearly the acidic properties of catalysts with their catalytic activity or selectivity. The divergence between the reports relating acidity with catalytic activity even in case of microporous zeolitic structures, for instance papers of Takahara et al. [13], Sheng et al. [14] and Zhang et al. [15], prompted us to undertake the detailed studies of acidity and porosity of hierarchical ZSM-5 ethanol dehydration catalysts. Thus the several different approaches of obtaining of hierarchical ZSM-5 zeolites were applied in this study.

The methods of the synthesis of hierarchical zeolites have been gathered around two main routes. *Bottom-up* methods at the stage of synthesis employ templates (e.g. surfactants, porous carbon, cationic polymers, etc.) [16-19] and zeolitization of mesoporous materials [20]. , or concern direct synthesis of nanosized crystals [21, 22]. Zeolitic systems obtained in the presence of surfactants contain the acid sites of high concentration and strength, and the additional uniform mesoporosity improves the accessibility of acid sites to reactants. The tuning of both the shape and size of pores is a matter of template strategy. Furthermore, appropriately designed bifunctional surfactants allowed exfoliation of zeolites and production of ‘ultrathin’ layers with thicknesses below 5 nm [23, 24]. Choi et al. showed [24] that ‘ultrathin’ zeolites demonstrate very high resistance against coke formation

because of facile diffusion of coke precursors from the internal acid sites. These 'ultrathin' ZSM-5 zeolite obtained by using diquaternary ammonium surfactant possessed external protonic sites of the strength lower than those situated inside micropores, but still higher than those formed in purely amorphous MCM-41.

On the other hand, a preferential extraction of the two main components of zeolites, i.e. silica (via desilication) [25-27] or alumina (via dealumination) [28] are the most common of *top-down* approaches. The extraction of aluminium atoms from framework led to the formation of zeolites with bimodal porosity; the steaming of zeolite Y is well-known example [29, 30]. Desilication has been reported as the one of the most effective approaches for obtaining the hierarchical zeolites [31]. The number of framework silicon atoms that could be removed without causing structural damage is governed by the features inherent to zeolites (Si/Al ratio and framework topology) as well as by the alkaline treatment conditions (type and concentration of desilicating agent used). Similarly to dealumination, desilication does not only create mesopores, but also affects the acidity of hierarchical zeolite mainly by modifying the nature of acidic sites [25, 32].

This work was attempted to offer a deep insight into acidity and porosity picture of novel micro/mesoporous ZSM-5 zeolites in respect to their catalytic performance in ethanol dehydration process. To the best of our knowledge the attempts of relating acidity or porosity to catalytic performance in ethanol dehydration process for production of DEE, C_2= and higher hydrocarbons were done in limited number. Furthermore, those studies based on significantly different zeolitic structures and various aluminium content offered only tentative conclusions in which catalytic activity in alcohols dehydration process has been attributed either to strong or weak acid sites [4, 13-15]. Thus the wide range of materials studied in this paper, from typically microporous ZSM-5 to micro/mesoporous analogues obtained by different methods, however representing at some points similar properties, allows following the influence of acidity and porosity on catalytic performance. Zeolites of similar aluminium content were obtained both by *bottom up* and *top down* approaches. The structural, textural and acidic properties of solely microporous bulk zeolite and its mesoporous counterparts were faced with their catalytic activity and selectivity to different products. Both the acidic picture and porosity properties, that were significantly perturbed by various synthesis and modification strategies, found clear reflection in catalytic performance of hierarchical zeolites described as volcano curve dependence.

2 Experimental

2.1 Studied Materials

Parent microporous ZSM-5 zeolite denoted as B-ZSM-5 of Si/Al = 32 was supplied by Zeolyst (CP 5524G). Desilication was carried out in the 0.1 M and 0.2 M solutions of NaOH&TBAOH (tetrabutylammonium hydroxide) mixture TBAOH/(NaOH+TBAOH) = 0.4 (samples denoted as D1-ZSM-5 and D2-ZSM-5, resp.) at the temperature of 80 ^{o}C for 5 hours. The 100 ml of solution was added to 3.0 g of zeolite. After desilication the suspension was cooled down in ice-bath, filtered and washed until neutral pH. Next a fourfold ion-exchange with 0.5 M NH_4NO_3 was performed at 65 ^{o}C for 1 hour. Finally, the zeolites were again filtered, washed with distillate water, dried overnight at room temperature and calcined at 550 ^{o}C.

Zeolites M1-ZSM-5 and M2-ZSM-5 of tuneable mesoporosity were obtained via a direct synthesis route using the amphiphilic organosilanes as a mesopore-directing agent [18]. For the synthesis of mesoporous zeolite M1-ZSM-5 of Si/Al = 29, the TPOAC (3-(trimethoxysilyl)propyl)octadecyldimethylammonium chloride) (Aldrich, 42 wt% in methanol) was added to a conventional ZSM-5 synthesis gel containing TPABr (tetrapropylammonium bromide). The molar synthesis composition was 43 Na_2O : 5 Al_2O_3 : 200 SiO_2 : 20 TPABr : 10 TPOAC :15 H_2SO_4 : 18000 H_2O. In a typical synthesis, 1.77 g NaOH, 2.75 g TPABr, 6.09 g TPOAC, and 130 g H_2O were dissolved in a polypropylene bottle. Then, 21.5 g TEOS (tetraethylorthosilicate) was added into the solution and stirred for 1 h. Then, 1.72 g $Al_2(SO_4)_3 \cdot 18H_2O$ dissolved in 37.0 g H_2O was added to the aforementioned solution and then homogenized by handshaking. The synthesis gel was stirred at room temperature for 24 h for aging. The resultant gel was hydrothermally treated in a tumbling autoclave at 130 ^{o}C for 240 h (M1-ZSM-5) or 170 ^{o}C for 72 h (M2-ZSM-5). After the hydrothermal crystallization, the precipitated products were filtered, washed with distilled water, dried at 110 ^{o}C and calcined at 550 ^{o}C [18].

Carbon-black templated zeolite (denoted as C-ZSM-5) was synthesized using the gel composition of 2.0 NaCl : 1.67 Al_2O_3 : 100 SiO_2 : 20 TPA_2O : 200 H_2O. The added carbon-black was 100 wt% of the added silica. In a typical synthesis, 0.69 g NaCl and 4.0 g aluminium isopropoxide were dissolved in 212 g TPAOH (tetrapropylammonium hydroxide) solution (TCI, 20 – 25% in H_2O). 122 g TEOS was added under vigorous stirring and the reaction mixture was stirred for 3 h at room temperature. Then, 35.2 g carbon black (HIBLACK 900L, Evonik, average particle size: 15 nm, surface area: 270 $m^2 g^{-1}$) was added and the mixture was stirred for 1 h for homogenization. The resultant mixture was heated at 90 ^{o}C on a hot plate under stirring to evaporate ethanol and extra H_2O to obtain the aforementioned gel composition. The resultant synthesis gel was transferred into a Teflon-lined stainless-steel autoclave and hydrothermally crystallized at 180 ^{o}C for 72 h. After cooling to room temperature, the zeolite product was filtered and washed thoroughly with deionized water. The product was dried in an oven at 130 ^{o}C and subsequently calcined in air at 600 ^{o}C for 6 h.

Ultrathin ZSM-5 analogue (denoted as U-ZSM-5) is built with the random assembly of thin 'flake-like' zeolite crystals anisotropically formed a 2-dimensional sheet-like structure with 2–6 nm thickness was synthesized according procedure given in the literature [23, 24]. Gemini-type quaternary ammonium surfactant with a formula of $C_8H_{17}–N^+(CH_3)_2–C_6H_{12}–N^+(CH_3)_2–C_8H_{17}$ was used as SDA. The starting molar composition was 1.25 Al_2O_3: 30 Na_2O: 100 SiO_2: 10 SDA: 24 H_2SO_4: 4000 H_2O. LUDOX HS-40 (40 wt. % suspension in H_2O, Aldrich) and aluminium sulfate octadecahydrate (98%, Aldrich)

were used as a silica and an aluminium source, respectively. The resultant gel was transferred into an autoclave and hydrothermally heated at 130 ^{o}C for 6 days under tumbling (60 rpm). The final product was filtered, washed with deionized water, dried at 120 ^{o}C and calcined at 500 ^{o}C for 5 h. To make an H^{+}-form, the calcined materials were ion-exchanged using 1 M NH_4NO_3 aqueous solution, followed by calcination at 500 ^{o}C [23, 24].

2.2 Characterisation Techniques

2.2.1 Chemical analysis

Si and Al concentrations in the parent and desilicated zeolites were determined by the ICP OES method with an Optima 2100DV (PerkinElmer) spectrometer.

2.2.2 X-ray diffraction (XRD)

Wide-angle XRD patterns were taken with a Rigaku Multiflex diffractometer equipped with Cu Kα radiation (40 kV, 40 mA).

2.2.3 Nitrogen sorption measurements at -196 ^{o}C

Low temperature nitrogen sorption measurements have been performed on a Quantachrome Autosorb-1-MP gas sorption system at -196 ^{o}C. Prior to the measurements, all samples have been degassed under high vacuum conditions for a duration of 16 h at 200 ^{o}C. The micropore volume has been calculated based on the t-plot method, while the Brunauer–Emmet–Teller (BET) method has been applied to determine the apparent specific surface area, taking into account the recommendations of Rouquerol et al. [33]. Distributions of mesopore diameters were calculated via the Barrett–Joyner–Halenda (BJH) algorithm using the adsorption branch [34].

2.2.4 QE-TPDA studies

QE-TPDA measurements of hexane, cyclohexane, n-nonane and 2,2-dimethyloctane (DMO) were performed using the apparatus and experimental procedures described in detail earlier [35]. Prior to the QE-TPDA experiment a sample (ca. 7 mg) was activated by heating in He flow (10 °C min^{-1} to 500 °C). The initial adsorption was carried out at room temperature by replacing pure helium used as the carrier gas with helium containing a small admixture of a hydrocarbon (ca. 0.5 vol%). After adsorption was completed, the QE-TPDA experiment was performed by cyclic heating and cooling the sample (10 °C min^{-1} to 400 °C or 2 °C min^{-1} to 150 °C) in He/hydrocarbon flow (6.5 cm^3min^{-1}). The desorption-adsorption cycles were separated by 1 h isothermal segments at room temperature. In the micro- and mesopore volume calculations, the experimental desorption maxima were integrated and related to the calibration data. Density of the adsorptive was assumed as equal to that of the liquid.

2.2.5 STEM investigations

The STEM micrographs were obtained using transmission electron microscope (JEOL 2100F) working at 200 kV, with Field Emission Gun (FEG), EDX analysis and STEM detectors for bright and dark mode.

2.2.6 IR studies

Prior to FTIR studies, the materials were pressed into the form of self-supporting discs (ca. 5-10 mg/cm^2) and pre-treated in situ in an IR cell at 500 ^{o}C under vacuum conditions for 1 hour. Spectra were recorded with a Bruker Tensor 27 spectrometer equipped with a MCT detector. The spectral resolution was of 2 cm^{-1}. All the spectra presented in this work were normalized to 10 mg of sample.

Total concentration of the Brønsted and Lewis acid sites in calibration materials was determined in quantitative IR studies of pyridine sorption according to the procedure described in refs [32, 36]. Pyridine was supplied by Sigma-Aldrich (≥ 99.8%).

The concentrations of the Brønsted acid sites accessible for bulky 2,6-di-*tert*-butylpyridine and pivalonitrile (hereafter denoted dTBPy and Pn, respectively) were also achieved from quantitative studies described in refs [37, 38], respectively.

The zeolites were contacted with dTBPy (≥97%, Sigma Aldrich) vapour at 170 ^{o}C, then physisorbed probe molecules were removed by evacuation at the same temperature. The concentration of the protonic sites detected by the dTBPy was calculated from the maximum intensities (the height) of the dTBPyH$^+$ bands at 1625 cm^{-1} and its extinction coefficient equal of 0.5 cm^{2}µmol^{-1}. The pivalonitrile (98%, Sigma Aldrich) was adsorbed on the zeolites at room temperature followed by 20 min. evacuation at the same temperature in order to remove the excess of physisorbed probe molecules. The concentration of the Brønsted and Lewis acid sites detected by the Pn was calculated from the maximum intensities of the respective bands at 2277 cm^{-1} and 2305 cm^{-1} and their extinction coefficient (0.11 and 0.15 cm^2·µmol^{-1}, resp.).

2.2.7 Catalytic tests: ethanol dehydration

Activities of the investigated samples were measured in ethanol dehydration in vapour phase. For each experiment, 0.05 g of fresh catalyst was mixed with 0.5 g of quartz grains and placed in a differential microreactor connected on line with a gas chromatograph. Reaction products were analysed using a PerkinElmer Clarus 580 equipped with Elite-Plot Q capillary column (30 m of length, 0.53 mm of inner diameter) and TCD detector. Prior the catalytic reaction the samples were standardized under continuous helium flow for 30 min at 300 ^{o}C. Then helium as a carrier gas was passed over the liquid ethanol obtaining the concentration of ethanol in helium flow 0.56 mmol /dm^3. The total flow rate of the feed stream was kept at 35 cm^3/min. The reaction temperature was changed from 100 to 300 ^{o}C. The space velocity in performed catalytic test was kept at 1.1 $g_{ethanol}/(g_{catalyst}\cdot h)$. The calculation of TOF (turnover frequency / s^{-1}) values was based on equation 1 given in ref. [39]:

$$\mathrm{TOF}\left(s^{-1}\right)=\frac{\text{Reactant flowrate}\left(\mu\text{mol s}^{-1}\right)\cdot\text{Conversion}}{\text{Quantity of sites}\left(\mu\text{mol g}^{-1}\right)\cdot\text{Catalyst weight (g)}} \qquad \text{eq. (1)}$$

The calculation of STY (site time yield / g·s^{-1}) values for a given product was based on equation 2 given in ref. [40]:

$$\mathrm{STY}\left(g\cdot s^{-1}\right)=\frac{\text{Reactant flowrate}\left(\mu\text{mols}^{-1}\right)\cdot\text{Yield}}{\text{Quantity of sites}\left(\mu\text{molg}^{-1}\right)} \qquad \text{eq. (2)}$$

3 Results and discussion

3.1 Structural and textural characterization

The XRD patterns of the bulk and carbon templated zeolites (B-ZSM-5 and C-ZSM-5, resp.) exhibited well resolved reflections representative for ZSM-5 structure (Fig. 1). Similar observation was made for the ultrathin zeolite (U-ZSM-5), slightly different proportion between the reflections intensity was assigned to different morphology of zeolite grains. In the case of typically mesoporous zeolites (M1-ZSM-5 and M2-ZSM-5) the XRD patterns confirmed formation of the ZSM-5 structure; however the lowered crystallinity was evidenced, especially well visible for zeolite M1-ZSM-5 of narrower mesopores. Lower crystallinity of M1-ZSM-5 zeolite was assigned to highly mesoporous structure of this material. The synthesis process leading to the generation of regularly distributed mesopores as small as 3-4 nm within the zeolite structure resulted in enhanced surface area, with high contribution of disordered mesopore surface. Similar effect was observed for M2-ZSM-5 zeolite with broader pore size distribution (Fig. 2), but still highly developed mesopore surface area. In the case of desilication procedure the XRD studies proved preservation of the crystalline structure upon alkaline treatment of D1-ZSM-5 and D2-ZSM-5 samples. The samples chosen for this study were characterized by similar Si/Al ratio in range between 23 and 36. This selection assured the ability to proper following the changes in catalytic performance related not only to acidity but also to porosity of samples (Tab. 1).

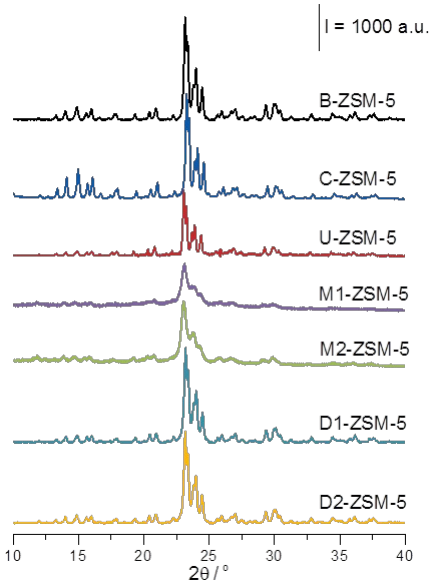

Figure 1 XRD patterns of studied materials

Table 1 The Si/Al ratio and the Al concentration determined by chemical analysis (Al_{ICP}), as well as the textural parameters from low temperature N_2 adsorption/desorption measurements for studied zeolites.

Material	Si/Al	Al_{ICP} [-/u.c.]	Al_{ICP} [µmolg^{-1}]	S_{BET} [m^{2}g^{-1}]	S_{meso} [m^{2}g^{-1}]	V_{micro} [cm^{3}g^{-1}]	V_{meso} [cm^{3}g^{-1}]
B-ZSM-5	32	2.91	471	377	40	0.17	0.06
C-ZSM-5	30	3.10	502	459	44	0.17	0.08
U-ZSM-5	36	2.59	420	555	250	0.16	0.41
M1-ZSM-5	29	3.20	518	603	250	0.11	0.48
M2-ZSM-5	29	3.20	518	520	187	0.16	0.35
D1-ZSM-5	27	3.43	556	322	85	0.11	0.16
D2-ZSM-5	23	4.00	648	405	185	0.10	0.32

Special attention was paid to the porosity studies of the investigated materials. In this aspect two experimental methods were applied: low-temperature nitrogen sorption and quasi-equilibrated

temperature programmed desorption of hydrocarbons (Section 3.2). As expected, the B-ZSM-5 zeolite demonstrated the type I N_2 adsorption isotherm (Fig. 2a) indicating presence of microporosity only, with V_{micro}=0.17 cm^3g^{-1} being the typical value for the MFI zeolite structure. Minor mesoporosity resulted from the interparticle space between the zeolite grains (Tab. 1). Similarly the N_2-isotherm for C-ZSM-5 zeolite was assigned to the type I, confirming microporous character of the sample. The STEM images of this zeolite show that the synthesis procedure does not allow to generate substantial mesoporosity, only the interparticle macroporosity can be present (Fig. 3).

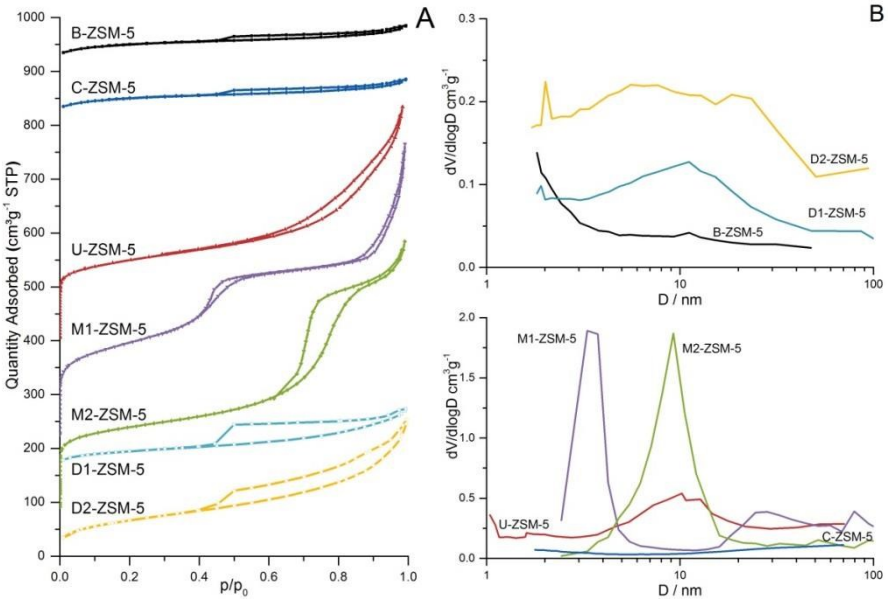

Figure 2 (a) Low temperature N_2 isotherms and (b) BJH pore size distributions of studied materials.

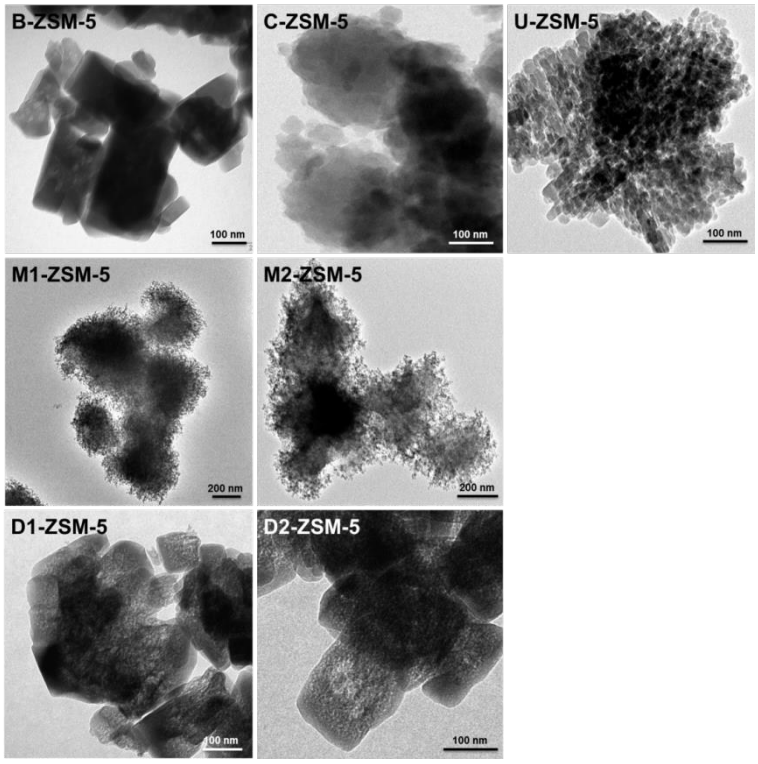

Figure 3 STEM images of bulk and micro/mesoporous zeolites

For the U-ZSM-5 sample exhibiting enhanced surface area due to the stacking of sheet-like zeolite structures, the PSD (Fig. 2b) indicated both the presence of mesopores and macropores. As mentioned earlier, the U-ZSM-5 material was obtained in directed synthesis with C_8–C_6–C_8 diquaternary ammonium surfactants. The use of gemini surfactants allowed the excessive growth of zeolite along the a and c-directions and random assembly of flake-like zeolite crystals. However, it cannot be excluded that the synthesised ultrathin zeolite is indeed a mixture of ultrathin and of nanosheets partially collapsed upon calcination, especially when the reflections between 10 and 20 ° 2θ occur in XRD pattern [23]. The STEM images confirm the porosity of the above mentioned materials and the sheet-like structure of U-ZSM-5 zeolite (Fig. 3).

Truly micro/mesoporous zeolites M1-ZSM-5 and M2-ZSM-5 showed a type-IV N_2-isotherms with steps accompanied by hysteresis loops at intermediate pressures, corresponding to the mesopores with 3.5 nm or 9.2 nm in diameter, resp., (Fig. 2b). Nevertheless, the lowered value of the micropore volume for M1-ZSM-5 zeolite suggests reduced crystallinity of this material. The STEM images of M1-ZSM-5 and M2-ZSM-5 zeolites (Fig. 3) demonstrated highly porous structure with small grains agglomerated in globular structures.

The D1-ZSM-5 and D2-ZSM-5 samples were representatives for alkaline treated zeolites. Despite the crystallinity preservation, the mesoporosity development upon alkaline treatment was found to be efficient enough. The alkaline leached materials demonstrated distinct mesoporosity development: while for the D1-ZSM-5 sample the S_{meso} reached only a moderate value, for D2-ZSM-5 S_{meso} value was close to that typical for mesoporous zeolite M2-ZSM-5. Worth underlining is the fact that for the alkaline treated samples the development of mesopore surface area occurred at the expense of micropore area. Similarly, the observed drop of V_{micro} was associated with an increase of V_{meso}. The STEM study (Fig. 3) confirmed the formation of mesopores inside the zeolite grains with interparticle character, different from the rest of presented mesoporous zeolites. The wide range of the materials studied, from typically microporous ZSM-5 to micro/mesoporous analogues obtained by different methods, however, representing at many points similar properties, allows following the influence of porosity character on catalytic performance.

3.2 QE-TPDA studies of porosity

The QE-TPDA method (Quasi Equilibrated Temperature Programmed Desorption and Adsorption) has been employed as a powerful experimental technique of porosity evaluation, complementary to low temperature nitrogen sorption. The QE-TPDA of volatile hydrocarbons is a novel experimental approach particularly designed for studying porosity of micro- and mesoporous materials [41]. It has been successfully applied in studies on zeolites, mesoporous silicas, their carbon replicas and metal-organic frameworks [42-45]. A QE-TPDA profile consists of desorption maxima observed during heating and adsorption minima while cooling the sample. In the QE-TPDA experiments desorption of *n*-alkanes from a porous sample is observed in temperatures 25-400 °C allowing detection of the micropores and mesopores, determination of their volume as well as the enthalpy and entropy of adsorption. Recently applied QE-TPDA measurements of 2,2-dimethyloctane (DMO) [35] allowed detection of the additional intermediate temperature maximum characteristic for a nanocrystalline ZSM-5, which was attributed to desorption of DMO molecules from the subsurface micropores with *n*-hexyl chains located inside the pore mouths and *t*-butyl groups protruding outside. Consequently, in this work the QE-TPDA method with use of DMO allowed following the changes in subsurface micropores while use of hexane and cyclohexane gave information on total microporosity. The aspect of developed mesoporosity was investigated with use of *n*-nonane, for which low temperature maxima, observed below 100 °C and resulting from desorption of the molecules filling the mesopores, can be applied for calculation of mesopore size distributions.

QE-TPDA profiles of hexane (Fig. 4) were found to be typical for the MFI type zeolites [41]. Characteristic two-step adsorption-desorption patterns resulted from the "commensurate freezing" effect, i.e. a kind of order-disorder transition of the adsorbed phase [46]. Lower intensity of the profile found for the desilicated and mesoporous samples (especially M1-ZSM-5 and D2-ZSM-5), together with additional low-temperature desorption contribution (observed immediately after commencement of heating the sample in desorption phase) indicated partial degradation of the zeolitic matrix, accompanied by increase of the external or mesopore surface area [47]. On the other hand, shapes of the profiles observed for the B-ZSM-5, C-ZSM-5 and U-ZSM-5 zeolites were characteristic for well-defined MFI framework.

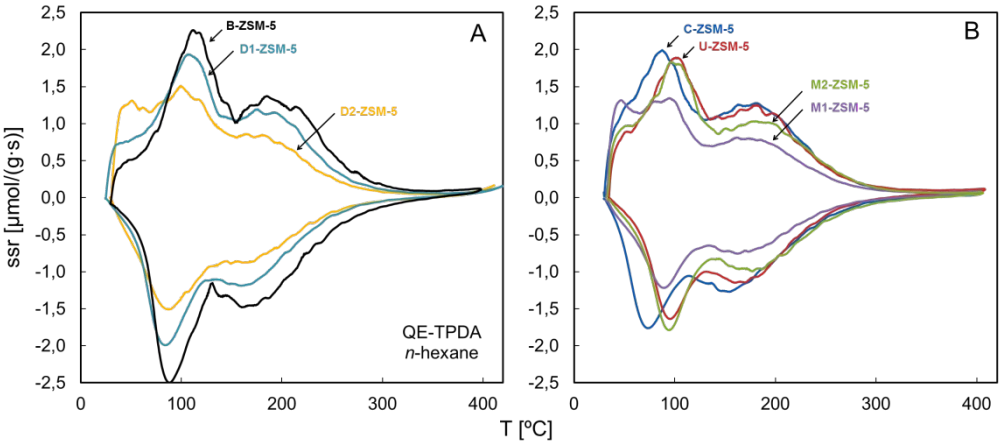

Figure 4 QE-TPDA profiles of *n*-hexane, recorded at 10°C/min.

Consistent results were obtained in QE-TPDA of cyclohexane (Fig. SI.1). Single desorption peak most probably should be attributed to the molecules located in the intersections of the channels of the MFI framework. Differences in the intensity and shape of these profiles confirmed some structural

imperfections in the desilicated, mesoporous and ultrathin zeolites. These imperfections were not observed for the bulk and carbon-templated materials.

The QE-TPDA profiles of *n*-nonane (Fig. SI.2a and SI.2b) consisted of low and high temperature features. The high temperature ones, corresponding to desorption from and adsorption in the micropores, respectively, showed similar differences as in previously discussed profiles of *n*-hexane and cyclohexane. The low temperature desorption and adsorption effects, related to the external surface and mesopores, were also studied in high resolution measurements with low heating and cooling rate (Fig. SI.2c and SI.2d). The low temperature desorption maxima differed considerably in their shape, intensity and positions. As they are much higher they indicated larger surface area and/or mesoporosity of the mesoporous (M1 and M2-ZSM-5), ultrathin (U-ZSM-5) and desilicated zeolites (D1 and D2-ZSM-5) than of the bulk (B-ZSM-5) and carbon-templated (C-ZSM-5) ones. The highest desorption temperature observed for the M1-ZSM-5 zeolite implies the lowest mesopore size.

These qualitative observations were fully supported by the mesopore size distributions calculated from the desorption (Fig. SI.3a and SI.3b) or adsorption (Fig. SI.3c and SI.3d) branches of the high resolution QE-TPDA profiles, according to a modified BJH scheme [45]. The PSDs obtained for the desilicated zeolites were typical for partially restricted, interconnected mesopore systems [48]. The sharp maxima at 4.5-4.7 nm, dominating desorption-based PSDs, did not correspond to real pore sizes, since they resulted from cavitation mechanism of emptying the mesopores leading to sudden release of the adsorbate. Better representation of porosity of D1-ZSM-5 and D2-ZSM-5 zeolites gave the adsorption-based PSDs, showing broad range of mesopore sizes. On the other hand, the PSDs with narrow and high peaks, obtained for M1-ZSM-5 and M2-ZSM-5 samples, show no desorption-adsorption hysteresis effects, thus revealing presence of highly uniform mesopores in these materials. Very broad and low-intensity maximum found for the ultrathin zeolite should be attributed to the interparticle mesopores formed between flat zeolitic layers. For the bulk zeolite only a limited amount of interparticle mesopores was found, while for the carbon-templated one essentially no mesoporosity was detected.

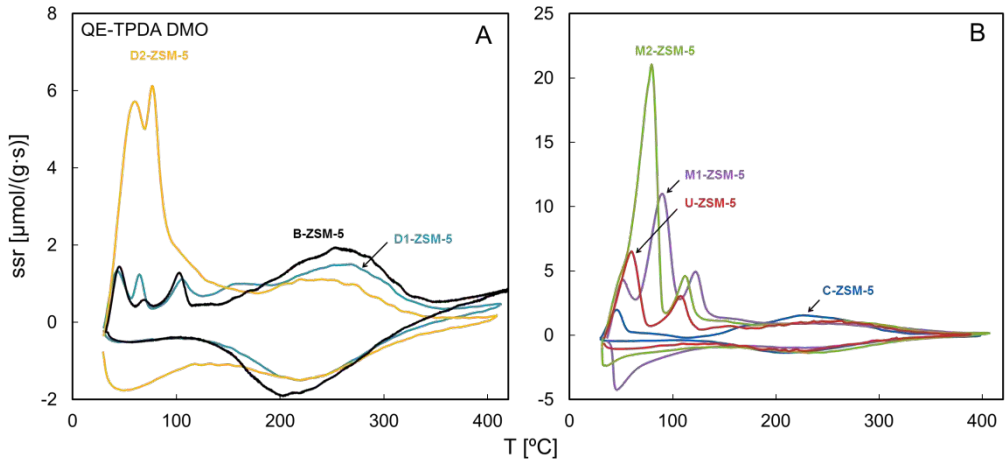

Figure 5 QE-TPDA profiles of DMO (2,2-dimethyloctane), recorded at 10°C/min.

The QE-TPDA profiles of DMO (Fig. 5a and 5b) were similar to that of *n*-nonane (Fig. SI.2a and SI.2b), apart from the additional desorption peaks at 100-120 °C. These maxima were attributed to the subsurface micropores, i.e. openings of 10-MR channels to the surface of ZSM-5 zeolites [35]. For DMO molecules adsorbed in these pores with the n-hexyl chains located inside and t-butyl groups

sticking out the interactions with the pore walls should be much weaker than those for the molecules fully contained within the micropores, resulting in lower desorption temperature. Only for C-ZSM-5 there was no such a peak in the QE-TPDA profile of DMO, indicating negligible amount or accessibility of subsurface micropores. Similarly, relatively high intensities of the middle temperature desorption peaks observed for all the other zeolites, suggested their comparable content of subsurface micropores.

Table 2 Values of the pore volume [cm^3g^{-1}] determined from the QE-TPDA profiles of hydrocarbons and adsorption isotherms of N_2

Material	nC_6	DMO		nC_9		N_2	
	V_{micro}	$V_{submicro}$	V_{meso}	V_{micro}	V_{meso}	V_{micro}	V_{meso}
B-ZSM-5	0.19	0.01	0.04	0.17	0.09	0.17	0.06
C-ZSM-5	0.17	0.00	0.06	0.16	0.09	0.17	0.08
U-ZSM-5	0.16	0.04	0.12	0.12	0.20	0.16	0.41
M1-ZSM-5	0.13	0.04	0.45	0.09	0.31	0.11	0.48
M2-ZSM-5	0.15	0.06	0.64	0.14	0.43	0.16	0.35
D1-ZSM-5	0.16	0.01	0.12	0.14	0.20	0.11	0.16
D2-ZSM-5	0.14	0.02*	0.37	0.15	0.37	0.10	0.32

**estimated after deconvolution of thermal curve*

Value of the pore volume calculated by integration of the desorption QE-TPDA peaks were listed in Table 2. The largest values of the micropore volume found from thermodesorption of hexane for B-ZSM-5 and C-ZSM-5 indicate that these materials consist only of well-defined MFI phase, while the lowest values observed for M1-ZSM-5 and D2-ZSM-5 can suggest distortion of the zeolitic framework and/or presence of nonporous amorphous silica. Similar results were found on basis of low temperature N_2 sorption experiments. However, it should be underlined that the lowering of micropore volumes in desilicated samples results rather from the presence of extra-framework material than loss of crystallinity, as indicated by XRD studies. The highest content of the subsurface micropores was found for the mesoporous (M1 and M2-ZSM-5) and ultrathin (U-ZSM-5) zeolites. High crystallinity of B-ZSM-5 and C-ZSM-5 was corroborated by very low mesopore volume determined from QE-TPDA profiles of DMO and *n*-nonane, attributed to interparticle mesopores. On the other hand, large values of the mesopore volume found for the mesoporous, ultrathin and desilicated zeolites are in line with completely different surface morphology expected for these materials. Worth noticing was distinctly lower mesopore volume of U-ZSM-5 zeolite in comparison to other micro/mesoporous zeolites. This result further supported conclusion derived from low temperature N_2 sorption studies that random assembly of thin 2–6 nm thickness flake-like zeolite crystals did not provide well-defined mesoporosity accessible to large hydrocarbon molecules. The correlation between the changes in textural parameters derived from QE-TPDA and acidic properties obtained from IR studies will be discussed afterword (Section 3.3.3).

3.3 IR acidity characterization

Modification of the textural parameters in each type of approaches of hierarchical zeolite formation inevitably alters their acidic properties. For this reason a detailed acidity characterization concerning the nature of acid sites, their strength, as well as their distribution between micropore and mesopore systems was performed by means of IR spectroscopy.

3.3.1 Analysis of the hydroxyls bands

The studied samples are characterized by the presence of hydroxyls groups of various origin and acidity (Fig. 6). The highest frequency band at 3745 cm^{-1} corresponds to the isolated silanols groups located on external surface of crystals and on mesopore surface that is significantly enlarged for the micro/mesoporous zeolites (D1-ZSM-5, D2-ZSM-5, M1-ZSM-5, M2-ZSM-5) (Tab. 1). The 3725 cm^{-1} band in zeolites B-ZSM-5 and C-ZSM-5 is attributed to the vicinal silanols. While the micro/mesopores zeolites (D1-ZSM-5, D2-ZSM-5, M1-ZSM-5, M2-ZSM-5) seem to be free of extra-framework non-acidic Al-species, the presence of 3690 cm^{-1} Al-OH band is easily detected in the bulk zeolite B-ZSM-5 and its ultrathin analogue U-ZSM-5. The significant intensity of the Al-OH band points to a low thermal stability of aluminium atoms in tetrahedral positions in zeolite U-ZSM-5.

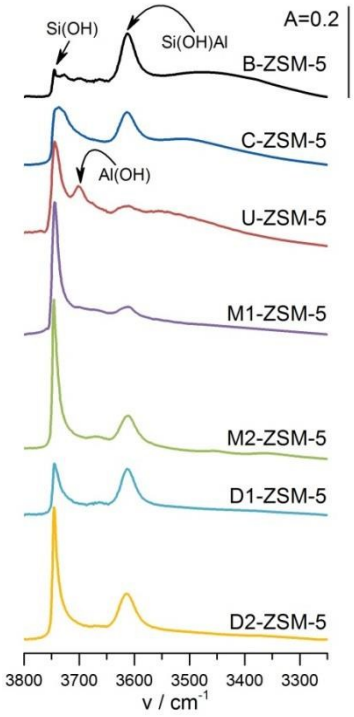

Figure 6 IR spectra of studied materials in the region of O-H vibration.

3.3.2 Concentration and strength of acid sites

The concentration of Brønsted and Lewis sites have been calculated using respectively the maximum intensities measured as the maximum height of the 1545 cm^{-1} band of pyridinium ions (PyH^+) and of the 1455 cm^{-1} band of coordinatively bonded pyridine to Lewis sites (PyL), by applying the extinction coefficients equal 0.07 $cm^2/\mu mol$ and 0.1 $cm^2/\mu mol$ [32, 36]. The results of quantitative studies of Py sorption were compared with Al concentration derived from chemical analysis (Tab. 3). The sum of Brønsted and Lewis acid sites concentrations are in line with the total Al concentration for all samples. Such observation implies that the main part of Al atoms is well dispersed and easily

accessible for pyridine molecule. What is more, the majority of Al atoms (76-97% of all Al atoms) generate the Brønsted acid sites, while the rest is source of the Lewis acidity or non-acidic Al-OH species. The changes in concentration of acid sites determined with use of Py as probe molecule found reflection in values of micropore area. For the microporous (B-ZSM-5, C-ZSM-5) and bottom-up modified zeolites (M1-ZSM-5, M2-ZSM-5, U-ZSM-5) the increasing acidity correlates with enhanced micropore area. The opposite effect is observed for the alkaline treated samples, from typically microporous B-ZSM-5 zeolite to alkaline treated (D1-ZSM-5, D2-ZSM-5) the increase of acidity is reflected in reduced microporous area (Fig. 7).

Table 3. Concentration ($\mu molg^{-1}$) of the Al determined by chemical analysis (Al_{ICP}), of the Brønsted (B) and Lewis (L) acid sites measured in quantitative experiments of pyridine (Py), pivalonitrile (Pn) and 2,6-di-*tert*-butylpyridine (dTBPy) sorption together with respective accessibility factors (AF_{Pn} and AF_{dTBPy}).

Material	Si/Al	Al_{ICP}	Py			Pn		AF_{Pn}			dTBPy	AF_{dTBPy}
			B	L	B +L	B	L	B	L	B+L	B	
B-ZSM-5	32	471	390	34	424	48	7	0.12	0.21	0.13	16	0.04
C-ZSM-5	30	502	390	100	491	38	18	0.10	0.18	0.11	15	0.04
U-ZSM-5	36	420	400	13	413	292	11	0.73	0.88	0.32	193	0.45
M1-ZSM-5	29	518	301	170	471	154	66	0.51	0.39	0.51	156	0.49
M2-ZSM-5	29	518	342	107	449	206	60	0.60	0.56	0.47	139	0.38
D1-ZSM-5	27	556	462	68	530	125	46	0.27	0.67	0.59	60	0.13
D2-ZSM-5	23	648	479	135	614	221	93	0.41	0.69	0.73	115	0.24

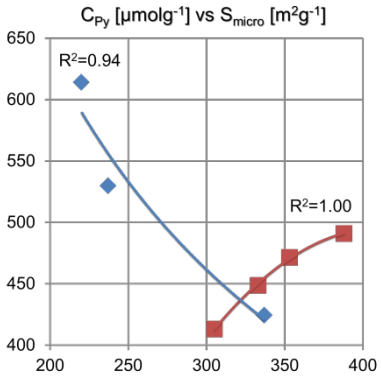

Figure 7 Dependence between the concentration of acid sites derived from Py sorption experiments and micropore area calculated from low temperature N_2 sorption for samples obtained from *bottom up* (■) and *top down* (◆) synthesis methods.

The total number of acid sites detected with pyridine corresponded with the aluminium content from chemical analysis, thus the diffusion of pyridine molecules at our experimental conditions was not limited even despite the high content of extra-framework species. The high concentration of Lewis acid sites in M1-ZSM-5 and D2-ZSM-5 zeolites was associated with some structural imperfection indicated by either lowered crystallinity of M1-ZSM-5 or distorted QE-TPDA profile of cyclohexane. Surprisingly, in the spectra of CO adsorbed on studied materials (Fig. 8) Lewis acid sites, originating from extra-framework aluminium (the 2197 cm^{-1} band) and dehydroxylation process (the 2230 cm^{-1} band) were detected for zeolites C-ZSM-5, D2-ZSM-5 and U-ZSM-5 only. No electron pair acceptor sites were found by CO in conventional B-ZSM-5 zeolite and hierarchical zeolites D1-ZSM-5, M1-ZSM-5 and M2-ZSM-5, in spite of their noticeable concentration in materials, as detected by Py sorption. This discrepancy can be related to different basicity of probe molecules; pyridine as stronger base [49, 50] was able to bond coordinatively to sites which were weak enough to exclude the bonding of CO molecule. Similar phenomenon has been observed for mesostructured zeolites obtained via desilication [32].

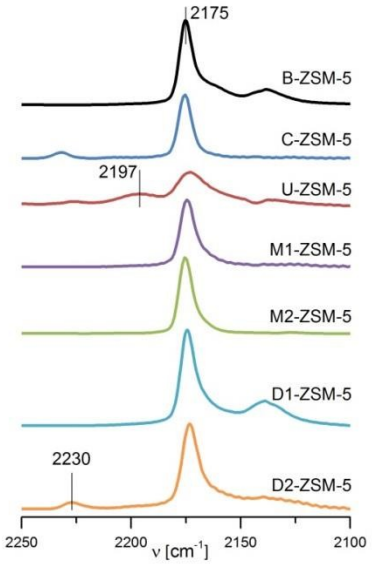

Figure 8 IR spectra of studied materials after CO sorption at -196 ^{o}C

Based on the IR data, information on the acid strength of protonic sites was derived from (i) the values of the $\Delta\nu_{OH..CO}$ obtained in CO sorption studies and (ii) pyridine thermodesorption experiments. Low temperature CO sorption experiments permitted determination of the downshift of the Si(OH)Al group band perturbed by hydrogen bonding with CO molecule, $\Delta\nu_{OH..CO}$. The more acidic Si(OH)Al groups are, the more pronounced downshift of the Si(OH…CO)Al bands is observed. Among the studied materials the highest $\Delta\nu_{OH..CO}$ values were revealed for typically microporous zeolites B-ZSM-5 and C-ZSM-5, thus the most acidic bridging hydroxyls were highly populated in those zeolites. Additionally, high value of $\Delta\nu_{OH..CO}$ was also obtained for U-ZSM-5 zeolite. The reduced acid strength of Si(OH)Al groups was observed for the rest of micro/mesoporous zeolites. In the Py-experiments, the conservation of the 1545 cm^{-1} (Brønsted sites) and 1450 cm^{-1} (Lewis sites) bands under the desorption procedure at 350 ^{o}C was taken as a measure of the acid strength of the acid sites (Tab. 4). Again, the microporous materials were of the highest contribution of the most acidic protonic sites. The exception was the ultrathin U-ZSM-5 zeolite where the population of strongly acidic Si(OH)Al is significantly reduced. This phenomenon is in line with literature reports and the external sites in nanosheets were recognized as less acidic than those in conventional solely microporous zeolite. Similar results have been demonstrated with use of solid-state ^{31}P MAS NMR spectroscopy of adsorbed trimethylphosphine oxide (TMPO) employed to probe Brønsted acid sites distribution in various zeolites [51, 52]. Furthermore, the protonic sites exposed on external surface of nanosheets were believed to be less strained from perfect tetrahedral geometry than in the internal zeolite framework sites, thus they acid strength was noticeably reduced [24]. The extensive solid acids characterization [53, 54] demonstrated that the ^{31}P chemical shift can be used to characterize the integrity of the zeolite micropores. The confinement effect resulting from long-range electrostatic effects of the Madelung potential in the zeolite framework has been successfully studied in case of ZSM-5 zeolites of various pore hierarchy [52, 55]. It has been showed that significantly more exposed acidic sites in the open mesopores are responsible for the decreased host/guest interactions and can easily fallowed by means of ^{31}P NMR spectroscopy [51]. The discrepancy between the results of CO and Py sorption again can be related to different basicity of probe molecules. Additionally, it has been reported that aluminium species, i.e. Lewis sites, existing on the mesopore surface, after the adsorption of strong bases such as ammonia or pyridine,

generated Brønsted acid site by bridging of a silanol over Al cation [56]. Thus, the amount of Brønsted sites detected by Py in mesoporous zeolites is always bigger that the amount of the Si(OH)Al groups probed by CO. In other words, total acidity of a zeolitic catalyst can be probed with a strong base but the acid strength of the Si(OH)Al bridging hydroxyls can be followed with a probe of low basicity only. It seems that this is especially important for U-ZSM-5 zeolite, since CO sorption experiments point out for higher strength of acid sites then Py thermodesorption results. Nevertheless, the employment of CO and Py as probes allowed for clear distinguishing of acid strength of sites in purely microporous and hierarchical materials. It has been shown that the development of mesopore surface area independently from the applied hierarchization methods leads to a materials possessing acid sites of lower strength.

Table 4. Acid strength of Brønsted sites measured as the downshift of the Si(OH)Al band perturbed by hydrogen bonding with CO molecule, $\Delta\nu_{OH..CO}$, as well as Brønsted and Lewis sites derived from Py-thermodesorption experiments.

Material	Acid strength of sites		
	$\Delta\nu_{OH...CO}$ [cm^{-1}]	Py	
		B	L
B-ZSM-5	315	0.95	1.00
C-ZSM-5	314	1.00	1.00
U-ZSM-5	313	0.70	1.00
M1-ZSM-5	311	0.89	1.00
M2-ZSM-5	312	0.90	1.00
D1-ZSM-5	312	0.91	1.00
D2-ZSM-5	310	0.85	1.00

3.3.3 Accessibility of protonic sites

With regard to catalytic applications, for a material with an ideal acidic properties the high concentration and strength of acid sites inherent to the bulk zeolite should meet the highest accessibility of acid sites to reagents. Differentiation between the overall concentration of acid sites and concentration of those located on the external surface of mesopores in typically microporous zeolites and micro/mesoporous zeolites obtained by "*top down*" and "*bottom up"* approaches was easily achieved using the hindered molecules as the probes [38, 47, 57, 58]. As mentioned earlier, the studied zeolites were obtained via "*bottom up"* approach in the presence of the amphiphilic organosilanes (M1-ZSM-5 and M2-ZSM-5) and gemini-type quaternary ammonium surfactant (U-ZSM-5) as mesopore-directing agents as well as by "*top down*" desilication process (D1-ZSM-5 and D2-ZSM-5). As the microporous analogues the commercially available zeolite (B-ZSM-5) and zeolite synthesized with use of carbon template (C-ZSM-5) were chosen. In general, all intentional approaches led to the generation of mesoporosity, i.e. the development of external surface area, thus shortened diffusion pathway for reactants. In the term of enhanced mesoporosity, dTBPy (2,6-di-*tert*-butylpyridine) [37] and Pn (pivalonitrile) [38] were employed as probe molecules delivering detailed characterization of accessibility of acid sites to reagent molecules in fully quantitative manner. The dTBPy (kinetic diameter *ca.* 1 nm), has been found as suitable probe for the quantitative investigation of the external acidity in hierarchically structured zeolites [37]. The dTBPy molecule is too large to enter the 10-MR micropores thus nearly no sites in non-mesoporous zeolites are detected by this probe. Consequently, dTBPy is able to selectively detect only the sites distributed on mesopore surface. The accessibility factor (AF_{dTBPy}) for the 2,6-di-*tert*-butylpyridine was defined as the number of sites detected by adsorption of the dTBPy (external sites) divided by the total amount of acid sites in the studied zeolites as quantified by pyridine sorption. The values of the accessibility factor (AF_{dTBPy}) are presented in Table 3. Additionally, Figure 9 presents the AF values in the

correlation with the mesopore surface in studied zeolites. As expected, nearly no sites in purely microporous zeolites B-ZSM-5 and C-ZSM-5 were detected by dTBPy molecules. However, after formation of a mesopore system the accessibility of Brønsted sites significantly raised reaching 50% of total amount of protonic sites detected by pyridine. Among the studied materials M1-ZSM-5 and U-ZSM-5 zeolites revealed the highest accessibility of protonic sites. This trend is in agreement with the development of mesopore surface.

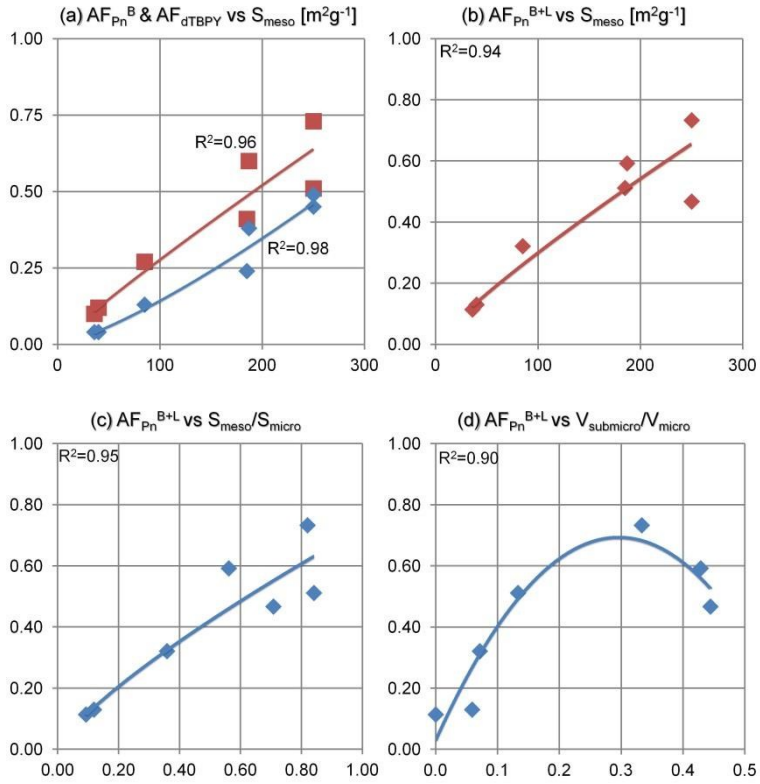

Figure 9 Accessibility factor values for (a) Brønsted acid sites and (b) sum of Brønsted and Lewis acid sites (AF_{dTBPy} – blue points, AF_{PN} – red points) plotted against mesopore surface area and accessibility factor values for sum of Brønsted and Lewis acid sites plotted against (c) the ratio of S_{meso}/S_{micro} from low temperature N_2 sorption and (d) the ratio of $V_{submicro}/V_{micro}$ from QE-TPDA studies

Contrary to dTBPy molecules probing solely protonic sites on mesopore surface, the pivalonitrile molecules are small enough to diffuse through the 10-MR channels at room temperature and reach the first available acid sites within the micropores in the subsurface region [38, 47]. Consequently, sorption of Pn allows quantifying the sites exposed on mesopore surface and those hidden near to micropore mouths. Additionally, sorption of Pn offers the possibility of distinguishing the Brønsted and Lewis acid sites. Similarly as for dTBPy, the values of the accessibility factors for pivalonitrile (AF_{Pn}) for Brønsted and Lewis acid sites were calculated as the ratio of the concentrations of acid sites accessible to Pn molecules to those determined from adsorption of pyridine (Tab. 3) and related to mesopore surface area of catalyst (Fig. 9). A comparison of the accessibility factors (AF) determined by different probe molecules (Tab. 3) showed that accessibility of Brønsted acid sites determined with pivalonitrile was significantly higher than accessibility to hindered dTBPy. The only exception is the M1-ZSM-5 material. Micropore entrances in this material were blocked by extra-framework Lewis sites formed during synthesis, as evidenced by low micropore volume, and the diffusion of pivalonitrile at room temperature was strongly limited. Since this imperfect crystalline structure, the same number of protonic sites interacted with both probes. The lower concentration

of Lewis acid sites in D2-ZSM-5 material resulted in less visible effect of pore blocking and higher accessibility of Brønsted acid sites to pivalonitrile than in the case of M1-ZSM-5 sample. For all the materials studied the accessibility factor values are highly correlated with mesopore surface area obtained from low temperature N_2 sorption experiments. Nevertheless, independently from kinetic diameter of probe molecule and type of acid sites being detected, the high dispersion of sites ensures enhancement of accessibility of acid sites with the increasing mesopore surface area (Fig. 9a, 9b and 9c). The increasing accessibility of acid sites related to their location on mesopore surface and/or external surface has been also demonstrated with use of ^{31}P NMR spectroscopy of TMPO (kinetic diameter 0.5 nm) in case of ZSM-5 zeolites of various pore hierarchy. The quantitative evaluation of the amount of acid sites located at external surfaces, related by authors with the ^{31}P peak in spectrum at approximately 50 ppm, allowed to correlate the changes in acidity of samples with their textural characteristics [51]. The valuable observations concerning accessibility of acid sites can be also done based on the QE-TPDA data obtained with DMO as probe molecule. The increase of the number of pore mouths expressed as $V_{submicro}$ [cm^3g^{-1}] only to some point led to increased accessibility of acid sites of given concentration (Fig. 9d). For samples M1-ZSM-5 and M2-ZSM-5 containing high amount of submicropores the accessibility factors AF_{Pn}^{B+L} represented almost the same values as for desilicated D2-ZSM-5 materials with significantly lower value of $V_{submicro}$. The total accessibility of acid sites can be reached only for materials characterized by either sufficiently high dispersion of sites or containing the amount of acid sites low enough so that each site could be reached through exposed pore mouth. This result found the confirmation in accessibility studies of acid sites in highly siliceous hierarchical ZSM-5 zeolite [38].

In alcohol dehydration reactions the active sites are supposed to be both Brønsted and Lewis acid sites [13, 14, 59]. Indeed, when both types of sites are detected, the reaction pathway involving Brønsted acid sites dominates [60]. However, the role of Lewis acid sites can not be ruled out as, besides that the dehydration of ethanol can occures over Lewis acid sites, the presence of these sites can enhance the Brønsted acidity or increase the stability of intermediates [61]. Furthermore the H^1 DQ-MAS NMR experiment and theoretical calculation demostrated that the Lewis acid sites in close proximity to Brønsted acid sites result in synergic effect that increase the acid strnegth of Brønsted acid sites [62, 63]. Therefore, the total accessibility factor as a function of mesopore surface area is also relevant. The linear correlation between the AF_{Pn}^{B+L} and mesopore surface area confirms increasing accessibility of acid sites with the development of mesoporosity. However, the observed lower accessibility of both types of acid sites in M1-ZSM-5 sample led to poor fitting of this result with the linear correlation observed for the rest of the samples (Fig. 9b). Similar observation were done for correlation between the AF_{Pn}^{B+L} and ratio of S_{meso}/S_{micro} which can be interpreted as textural parameter defining the progress of mesoporosity development in studied zeolites (Fig. 9c).

3.4 Catalytic performance in ethanol dehydration

The catalytic activity of the investigated zeolites samples in dehydration of ethanol in the vapour-phase was studied at the temperatures ranging from 100 ^{o}C to 300 ^{o}C and atmospheric pressure, with space velocity equal to 1.1 h^{-1}. Prior to the catalytic test the samples were in situ heated at 300 ^{o}C for 30 min to remove water from zeolite channels. The reaction conditions was adjusted to differentiate between the micro and micro/mesoporous catalysts, thus the relatively high flow rate and the low amount of catalyst used ensured that their activity is not overestimated. The catalytic performance of the hierarchical materials was compared with the bulk zeolite with regard to the type of generated mesoporosity and retained acidity. The attempts of correlating the acidity of catalysts with their performance published till now were based only on the results of NH_3TPD method attributing strong [13] or weak [39] acid sites to be active, or failed to found any relationship [59]. The valuable correlation between catalytic results of DEE synthesis from ethanol and acidic characteristic of Brønsted sites in zeolites was obtained from in situ chemical titration with use of dimethyl ether [4]. However, the in situ assessment of the role of Lewis acidity in catalytic reactions involving also these centres (e.g. ethylene and higher hydrocarbons synthesis) is still an open issue. Another important factor of hydrocarbon transformations over zeolites that has a strong effect on adsorption state, reaction mechanism and reactivity of the hydrocarbon transformation, thus finally on catalytic performance, is the pore confinement effect imposed by the zeolite framework [64].

Micro/mesostructured zeolites were catalytically active at the temperature range of ca. 200-300 ^{o}C where diethyl ether and ethylene were two main products competitively formed at atmospheric pressure. Figure 10 represents the relationship between conversion, selectivities, yields and the reaction temperature. The conversion of ethanol (Fig. 10a) increases sharply with the increasing reaction temperature for all samples reaching 100% at 280-320 ^{o}C. Within the whole range of reaction temperature the highest conversion of ethanol was observed for C-ZSM-5 and it was found to decrease in the following order: C-ZSM-5 > B-ZSM-5 ≈ U-ZSM-5 > D1-ZSM-5 > D2-ZSM-5 ≈ M2-ZSM-5 > M1-ZSM-5. The most effective catalysts were those representing the well-defined micropore structure (B-ZSM-5, C-ZSM-5) or, as in the case of U-ZSM-5 zeolite, possessing the enhanced accessibility reaching nearly 75 % of acid sites, but still presenting mostly microporous characteristics. The lowest catalytic activity was recognized for M1-ZSM-5 what is in line with limited crystallinity and poorly preserved microporous structure. At this point it can be seen that catalytic activity of microporous zeolites (B-ZSM-5, C-ZSM-5) and U-ZSM-5 zeolite was distinctly higher than activity of samples containing precisely defined porosity (D1-ZSM-5, D2-ZSM-5, M-1-ZSM-5, M2-ZSM-5), being evidenced by values of TOF (turnover frequency / s^{-1}) and STY (site time yield / $g{\cdot}s^{-1}$) (Tab. 5). With this in mind, the correlation of the conversion with intrinsic acidity of zeolites expressed as difference between concentration of acid sites detected with use of Py (total acidity) and Pn (external acidity) ($C_{Py} - C_{Pn}$ / $\mu molg^{-1}$) (Fig. 11a) seems to be obvious conclusion. Catalytic behaviour of Brønsted acid sites in materials with dual meso-/microporosity was previously demonstrated as being dominated by the microporous environment, what was assigned to better fit for adsorption of small alkane or alcohol reactant molecules [4]. Further discussion will be based on catalytic parameters dependence on accessibility factor AF_{Pn}^{B+L}, representing the percentage of sites available from the external and subsurface region. Consequently, the correlation of both the conversion and the TOF/STY values with the accessibility of acid sites measured as AF_{Pn}^{B+L} (Fig. 11) has been also found. It is not surprising because the development of mesoporosity, thus the increase of the amount of external sites, occurs at the expense of intrinsic acidity.

Also the product yields were considered as equally important estimates of catalytic performance (Fig. 10b, d and f). The catalytic performance of ZSM-5 zeolite with respect to the yield of different products can be directly considered in the terms of both accessibility and strength of acid sites. The highest yield of DEE equal to 64 % was observed for C-ZSM-5 sample at the temperature of 220 °C. The C-ZSM-5 exhibited also the highest yield to ethylene and C_{3+} products. For micro/mesoporous zeolites the temperature of 300 °C was demanded to reach more than 80 % of $C_{2=}$ yield. Both diethyl ether and ethylene are products of reactions typical of catalysts characterized by acid sites, however strong intrinsic acid sites in the catalysts favour hydrocarbons formation by ethylene polymerization [7]. Indeed, the yield of C_{3+} products (at temperatures above 280 °C) is significantly higher for all microporous type zeolites C-ZSM-5, B-ZSM-5 and U-ZSM-5 being fully justified by well-developed micropore environment (Fig. 10d). For U-ZSM-5 zeolite the DEE and $C_{2=}$ yields allow for conclusion that the mesoporosity of this material does not significantly affect its catalytic performance.

Table 5 Site time yields [10^{-4} g·s^{-1}] and turnover frequency [10^{-4} s^{-1}] values for studied catalysts in different temperatures of reaction

Material	140 °C		220 °C		240 °C		**260 °C**	
	STY_{DEE} /10^{-2} g·s^{-1}	TOF_{DEE} /10^{-2} s^{-1}	STY_{DEE} /10^{-2} g·s^{-1}	STY_{C2} /10^{-2} g·s^{-1}	STY_{DEE} /10^{-2} g·s^{-1}	STY_{C2} /10^{-2} g·s^{-1}	**STY_{DEE} /10^{-2} g·s^{-1}**	**STY_{C2} /10^{-2} g·s^{-1}**
B-ZSM-5	0.11	2.27	4.68	0.26	1.92	4.04	6.22	1.53
C-ZSM-5	0.15	2.96	4.32	0.43	0.11	5.26	4.87	1.83
U-ZSM-5	0.05	1.00	3.07	0.06	3.21	1.41	5.21	0.99
M1-ZSM-5	0.02	0.46	2.14	0.03	3.01	0.85	4.48	0.89
M2-ZSM-5	0.00	0.08	1.71	0.02	3.94	0.57	4.80	0.69
D1-ZSM-5	0.03	0.63	2.93	0.04	4.12	1.07	6.23	1.07
D2-ZSM-5	0.14	2.88	4.54	0.25	1.78	4.31	6.53	1.45

The effect of reaction temperature on the selectivities to diethyl ether (DEE), ethylene ($C_{2=}$) and higher hydrocarbons (C_{3+}) is presented in Figure 10c, e and g. As mentioned earlier, simultaneously with the reaction temperature the increase of ethanol conversion is observed, and the selectivity to ethylene being the product of an endothermic reaction becomes dominant [65]. Still the positive effect observed for micro/mesoporous zeolites on selectivity to DEE can result from the lowered strength of acid sites (Tab. 4) and facile diffusion enabling the formation of more branched DEE product. As formation of bulkier ethanol dimers is energetically more favourable the micro/mesoporous character of the zeolites and lower strength of the acid sites further enhance the selectivity to DEE [66]. The highest selectivity to DEE as exothermic reaction product was recognized for all types of the micro/mesoporous zeolites (D1-ZSM-5, D2-ZSM-5, M1-ZSM-5, M2-ZSM-5). At the same time, at the temperatures higher than 250 °C (for C-ZSM-5 > B-ZSM-5 ≈ U-ZSM-5) and 270 °C (D1-ZSM-5 > M2-ZSM-5 > D2-ZSM-5 > M1-ZSM-5) the selectivity to $C_{2=}$ increases and formation of ethylene becomes dominating. The highest selectivity for C_{3+} products is observed for C-ZSM-5 and decreases in following order: C-ZSM-5 > U-ZSM-5 ≈ B-ZSM-5 > D1-ZSM-5 > M2-ZSM-5 > D2-ZSM-5 > M1-ZSM-5. The order of decreasing C_{3+} selectivity is the same which was noticed for the catalytic activity. The formation of C_{3+} products is preferential for zeolites with the highly developed micropore system, what further supports fact that the confinement effect and high acid strength has significant influence on reactions involving C-C bond formation. The better developed or preserved micropore structure and the higher acid strength the formation of C_{3+} products occurs in lower temperatures. The reduced $C_{2=}$ and C_{3+} selectivity dependence on AF_{Pn}^{B+L} values should be most probably ascribed to differences in acidic character required to proceed the dehydration and oligomerizations reactions responsible for the formation of respective products. The dehydration of ethanol can take please on acid sites of all range of strength, while the bond formation reactions strongly depend on the presence of strong Brønsted acid sites [67]. The influence of acid strength

and confinement effect on the ethylene dimerization reaction over zeolites has been extensively studied by advanced methods [64, 68]. The long range electrostatic and van der Waals interaction between the zeolite framework and hydrocarbon fragments can be responsible for additional stabilizing effect on the confined species. It has been shown by theoretical studies that the activation energies for zeolite catalysed dimerization of ethylene decreased when extended zeolite framework models have been considered [68]. Furthermore, the stability of intermediate species in zeolite framework depend on both electrostatic and repulsive interaction between confined hydrocarbon fragments and zeolite framework [64], thus it can be supposed why the various pore hierarchy found reflection in activity and selectivity of herein studied zeolites. The reaction mechanisms of ethanol dehydration and consequent oligomerization are still a matter of debate. The dehydration of ethanol to DEE or ethylene is assigned by J.N. Kondo et al. [69, 70] to proceed by concerned mechanism, however the stepwise mechanism is also well supported by advanced theoretical studies [64, 68]. Still however, regardless of the temperature, the accessibility of acid sites expressed as AF_{Pn}^{B+L} seems to affect the selectivity of all products, favouring the formation of those which are energetically preferable (Fig. 12). The changes of selectivities to different products follow the volcano type curve with the micro/mesoporous samples located at its maximum or minimum depending on the product type. The specific shape of curve suggests that optimal values of conversion, STY and selectivities at particular temperature can be tuned by the amount of acid sites in microporous environment, thus located in microporous and subsurface region.

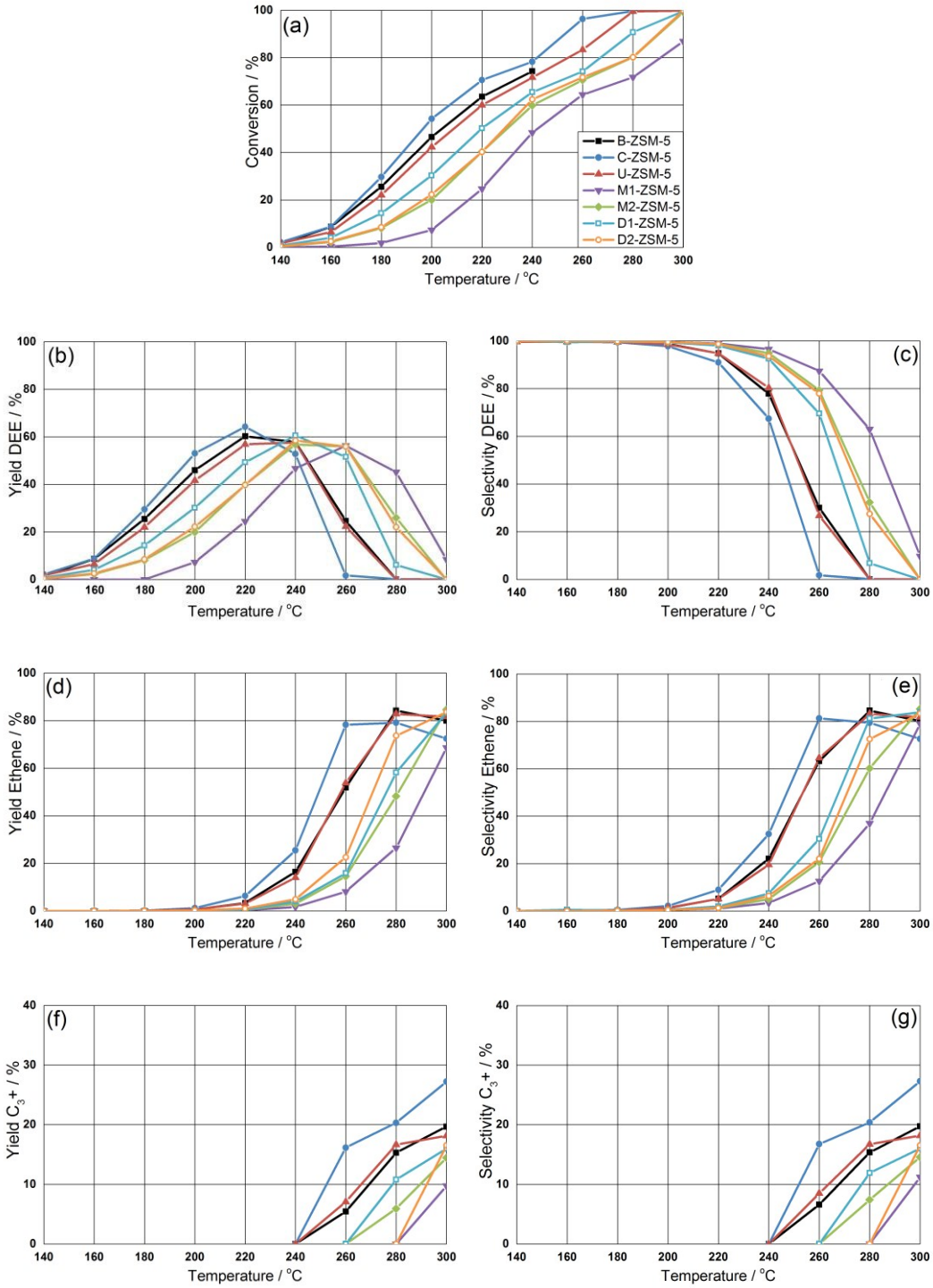

Figure 10 (a) Conversion of ethanol, (b, d, f) yields and (c, e, g) selectivities to diethyl ether, ethylene and higher hydrocarbons (C_{3+}) over B-ZSM-5 (■),C-ZSM-5 (●), U-ZSM-5(▲),M1-ZSM-5 (▼), M2-ZSM-5 (◆), D1-ZSM-5 (□) and D2-ZSM-5 (○) catalysts

Clear difference between the microporous and micro/mesoporous samples regarding the catalytic activity and selectivity is observed. The only exception is the U-ZSM-5 zeolite with enhanced mesopore surface area still presenting superior activity and selectivity to $C_{2=}$ typical for the microporous B-ZSM-5 zeolite. The structural and textural properties of the U-ZSM-5 sample suggest that highly enlarged surface area results from the presence of stacking of sheet-like zeolite structures and presence of macropores. Well-developed microporosity confirmed by high V_{micro} followed by high degree of grains agglomeration account for prevalent microporous character of this sample

during its catalytic performance. The confirmation of the microporous nature of the U-ZSM-5 zeolite in its catalytic performance can be seen also in the selectivity to C_{3+} products, which is roughly the same as for B-ZSM-5 zeolite.

It is known that deactivation of zeolite type catalysts can result from acid sites poisoning and/or pore blocking by accumulation of carbonaceous deposits. However, in this case we have not observed any deactivation of investigated catalysts during higher hydrocarbons formation. The higher amounts of C_{3+} products are formed over zeolites evidencing highly defined microporous character, i.e. B-ZSM-5, C-ZSM-5 and U-ZSM-5.

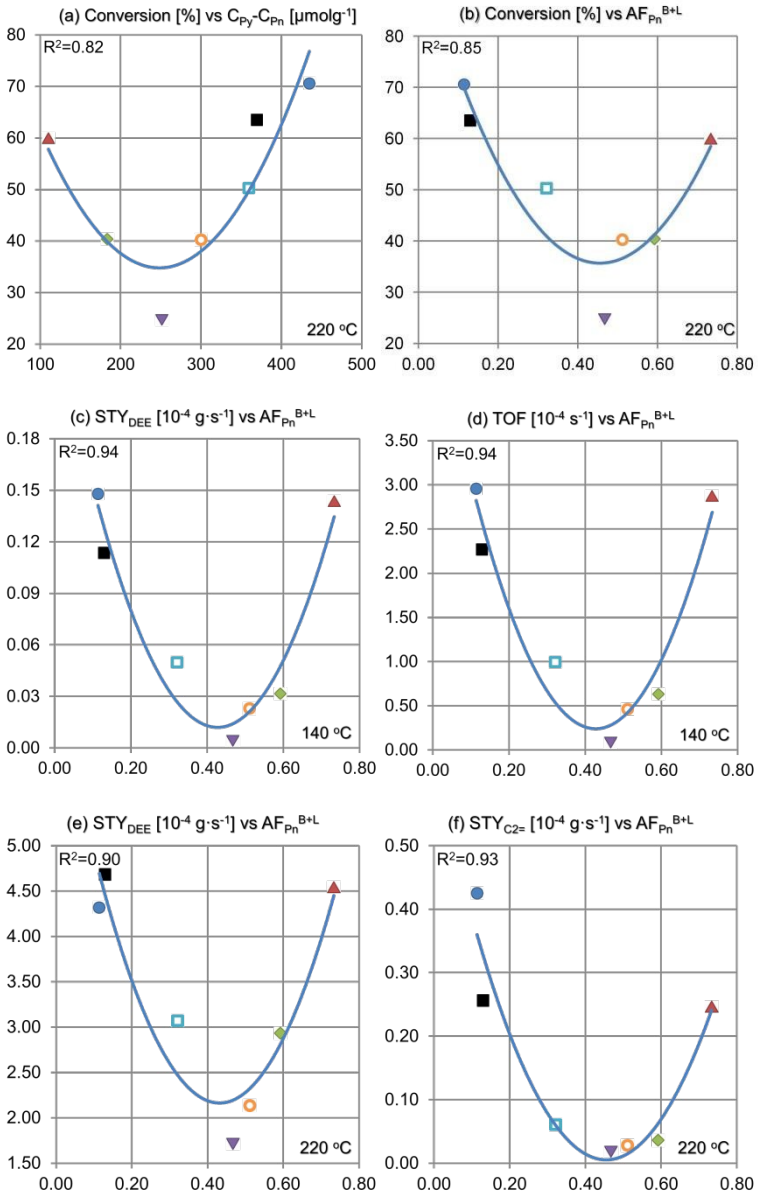

Figure 11 Conversion [%] and TOF [10^{-4} s^{-1}] and STY [10^{-4} g·s^{-1}] values obtained at reaction temperatures of 140 °C and 220 °C plotted against concentration of intrinsic acidity expressed as $C_{Py} - C_{Pn}$ and/or against the values of accessibility factor for both Brønsted and Lewis acid sites AF_{Pn}^{B+L} for studied zeolites B-ZSM-5 (■),C-ZSM-5 (●), U-ZSM-5(▲),M1-ZSM-5 (▼), M2-ZSM-5 (◆), D1-ZSM-5 (□) and D2-ZSM-5 (○)

Concluding, all aspects of catalytic performance of the studied zeolites were affected by the accessibility of acid sites expressed as AF_{Pn}^{B+L} (Fig. 11 and 12). Similarly as in the case of conversion and STY values the selectivities to different products of ethanol dehydration were found to be

depended on AF_{Pn}^{B+L} and strength of acid sites (Tab. 4). Our results strongly support conclusion that for catalytic reactions involving small hydrocarbons and their transformations both the microporous character and intrinsic acidity of zeolites seem to be crucial [11, 12, 71, 72]. Similar conclusion has been drawn also by Khare et al. [73] who correlated total light olefin selectivity over ZSM-5 zeolites in MTH reaction with the effective crystallite size. The better developed micropore area (quality of microporous character) and intrinsic acidity are, the higher catalytic activity in this type of reaction. In other words, the microporous character predominates catalytic performance for reactions undergoing without space limitations. The mesoporosity is responsible for enhanced accessibility of larger molecules [4] and enhanced lifetime of the catalyst. Thus, balancing between the microporous and mesoporous environment of the catalyst is decisive factor for its activity and lifetime.

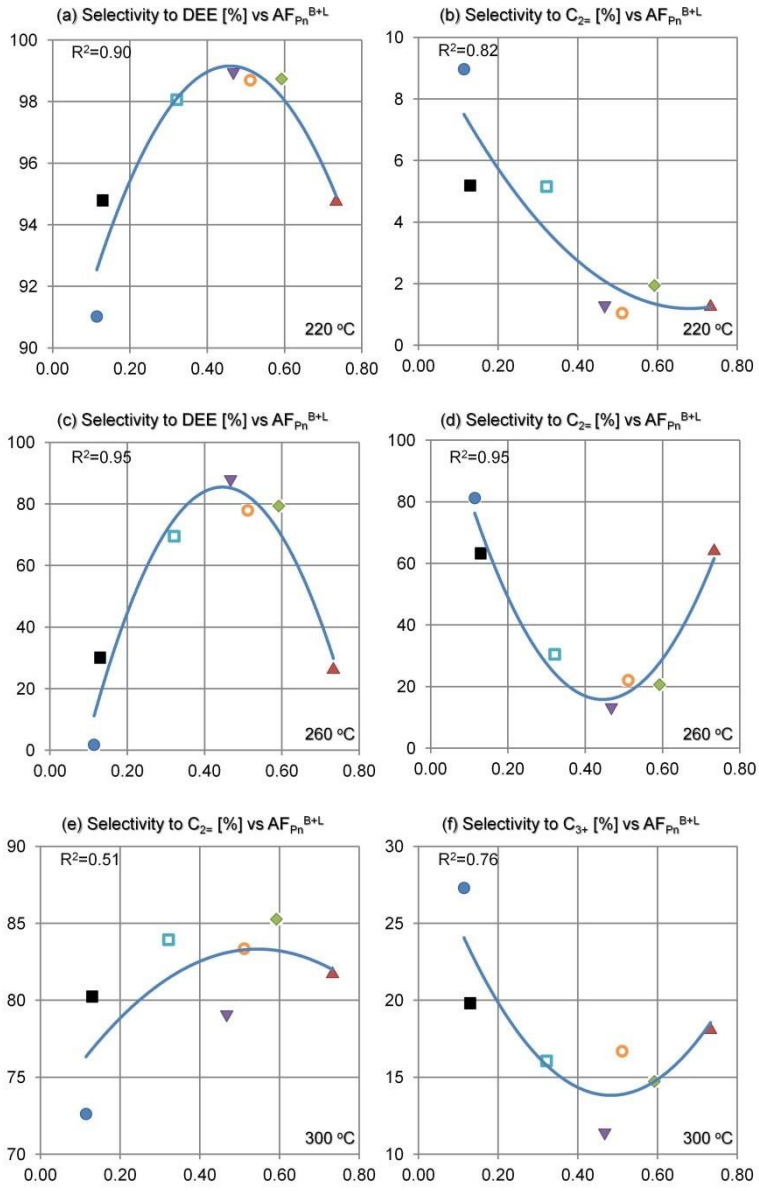

Figure 12 Selectivity of catalysts B-ZSM-5 (■),C-ZSM-5 (●), U-ZSM-5(▲),M1-ZSM-5 (▼), M2-ZSM-5 (◆), D1-ZSM-5 (□) and D2-ZSM-5 (○) to DEE, $C_{2=}$ and C_{3+} products in different temperatures plotted against values of accessibility factor of acid sites (B+L).

4 Conclusions

In the course of the ethanol dehydration reaction the acidity and the porosity picture of novel micro/mesoporous ZSM-5 zeolites have a significant influence on catalysts performance. All aspects of the catalytic performance of the investigated zeolites were affected by accessibility of acid sites expressed as the accessibility factor combining both Brønsted and Lewis type acidity. Particularly the selectivities to different products were found to be dependent on the accessibility factor and strength of the acid sites. It has been proven that the better developed micropore area and intrinsic acidity are, the higher catalytic activity and selectivity to ethylene are observed. Furthermore, it can be concluded that in the catalysts designing there is a need for balancing between the microporous and the mesoporous character of catalysts as the former is responsible for its activity and the latter is decisive for its lifetime.

Author Contributions

The manuscript was written through contributions of all authors. All authors have given approval to the final version of the manuscript.

Acknowledgement

This work was financed by Grant No. 2013/09/B/ST5/00066 from the National Science Centre, Poland.

References

1. M. Zhang, Y. Yu, Ind. Eng. Chem. Res. 52 (2013) 9505-9514.

2. T. Kito-Borsa, D.A. Pacas, S. Selim, S.W. Cowley, Ind. Eng. Chem. Res. 37 (1998) 3366-3374.

3. C.B. Phillips, R. Datta, Ind. Eng. Chem. Res. 36 (1997) 4466-4475.

4. D. Liu, A. Bhan, M. Tsapatsis, S. Al Hashimi, ACS Catal. 1 (2011) 7–17.

5. T. Zaki, J. Coll. Inter. Sci. 284 (2005) 606-613.

6. F.F. Madeira, H. Vezin, N.S. Gnep, P. Magnoux, S. Maury, N. Cadran, ACS Catal. 1 (2011) 417-424.

7. Y. Chen, Y. Wu, L. Tao, B. Dai, M. Yang, Z. Chen, X. Zhu, J. Ind. Eng. Chem. 16 (2010) 717-722.

8. A. Ciftci, D. Varisli, K. Cem Tokay, N. Aslı Sezgi, T. Dogu, Chem. Eng. J. 207–208 (2012) 85-93.

9. D. Varisli, T. Dogu, G. Dogu, Chem. Eng. Sci. 62 (2007) 5349-5352.

10. J. Bi, X. Guo, M. Liu, X. Wang, Catal. Today 149 (2010) 143-147.

11. L. Lakissa, F. Ngoye, Y. Pouilloux, Z. Qin, M. Tarighi, K. Thomas, V. Valtchev, L. Pinard, J.-P. Gilson, J. Catal. 328 (2015) 165–172.

12. M. Bjørgen, F. Joensen, M. Spangsberg Holm, U. Olsbye, K.-P. Lillerud, S. Svelle, Appl. Catal. A: Gen. 345 (2008) 43-50.

13. I. Takahara, M. Saito, M. Inaba, K. Murata, Catal. Lett. 105 (2005) 249-252.

14. Q. Sheng, K. Ling, Z. Li, L. Zhao, Fuel Proc. Tech. 110 (2013) 73-78.

15. D. Zhang, R. Wang, X. Yang, Catal. Lett. 124 (2008) 384-391.

16. Y. Liu, W. Zhang, T.J. Pinnavaia, Angew. Chem. Int. Ed. 40 (2001) 1255-1258.

17. I. Schmidt, A. Boisen, E. Gustavsson, K. Ståhl, S. Pehrson, S. Dahl, A. Carlsson, C.J.H. Jacobsen, Chem. Mater. 13 (2001) 4416-4418.

18. M. Choi, H.S. Cho, R. Srivastava, C. Venkatesan, D.-H. Choi, R. Ryoo, Nat. Mater. 5 (2006) 718-723.

19. H. Wang, T.J. Pinnavaia, Angew. Chem. Int. Ed. 45 (2006) 7603-7606.

20. I.I. Ivanova, E.E. Knyazeva, Chem. Soc. Rev. 42 (2013) 3671-3688.

21. S. Mintova, J.-P. Gilson, V. Valtchev, Nanoscale 5 (2013) 6693-6703.

22. C.J. Van Oers, K. Gora-Marek, K. Sadowska, M. Mertens, V. Meynen, J. Datka, P. Cool, Chem. Eng. J. 237 (2014) 372-379.

23. M. Choi, K. Na, J. Kim, Y. Sakamoto, O. Terasaki, R. Ryoo, Nature 461 (2009) 246-249.

24. K. Kim, R. Ryoo, H.-D. Jang, M. Choi, J. Catal. 288 (2012) 115-123.

25. K. Sadowska, K. Gora-Marek, M. Drozdek, P. Kustrowski, J. Datka, J. Martinez Triguero, F. Rey, Micropor. Mesopor. Mater. 168 (2013) 195-205.

26. D. Verboekend, M. Milina, S. Mitchell, J. Pérez-Ramírez, Cryst. Growth Des. 13 (2013) 5025-5035.

27. S. Abelló, A. Bonilla, J. Pérez-Ramírez, Appl. Catal. A: Gen. 364 (2009) 191-198.

28. M. Müller, G. Harvey, R. Prins, Micropor. Mesopor. Mater. 34 (2000) 135-147.

29. R.A. Beyerlein, G.B. McVicker, L.N. Yacullo, J.J. Ziemiak, J. Phys. Chem. 92 (1988) 1967-1970.

30. D.C. Koningsberger, J.T. Miller in Stud. Surf. Sci. Catal., ed. J.W. Hightower, W.N. Delgass, E. Iglesia, A.T. Bell, Elsevier, 1996, vol. 101 pp. 841-850.

31. D. Verboekend, J. Pérez-Ramírez, Catal. Sci. Tech. 1 (2011) 879-890.

32. K. Sadowska, K. Góra-Marek, J. Datka, Vib. Spec. 63 (2012) 418-425.

33. J. Rouquerol, P. Llewellyn, F. Rouquerol, in Stud. Surf. Sci. Catal., ed. P.L. Llewellyn, F. Rodriquez-Reinoso, J. Rouqerol, N. Seaton, Elsevier, 2007, vol. 160, pp. 49-56.

34. E.P. Barrett, L.G. Joyner, P.P. Halenda, J. Am. Chem. Soc. 73 (1951) 373-380.

35. W. Makowski, K. Mlekodaj, B. Gil, W.J. Roth, B. Marszalek, M. Kubu, P. Hudec, A. Smieskova, M. Hornacek, Dalton Trans. 43 (2014) 10574-10583.

36. K. Góra-Marek, M. Derewiński, P. Sarv, J. Datka, Catal. Today 101 (2005) 131-138.

37. K. Góra-Marek, K. Tarach, M. Choi, J. Phys. Chem. C 118 (2014) 12266-12274.

38. K. Sadowska, K. Góra-Marek, J. Datka, J. Phys. Chem. C 117 (2013) 9237-9244.

39. H. Xin, X. Li, Y. Fang, X. Yi, W. Hu, Y. Chu, F. Zhang, A. Zheng, H. Zhang, X. Li, J. Catal. 312 (2014) 204-215.

40. M. Boudart, Chem. Rev. 95 (1995) 661-666.

41. W. Makowski, Thermochim. Acta 454 (2007) 26-32.

42. W. Makowski, P. Kuśtrowski, Micropor. Mesopor. Mater. 102 (2007) 283-289.

43. W. Makowski, M. Leżańska, M. Mańko, J. Włoch, J. Porous Mater. 17 (2010) 737-745.

44. W. Makowski, M. Mańko, P. Zabierowski, K. Mlekodaj, D. Majda, J. Szklarzewicz, W. Łasocha, Thermochim. Acta 587 (2014) 1-10.

45. W. Makowski, L. Chmielarz, P. Kuśtrowski, Micropor. Mesopor. Mater. 120 (2009) 257-262.

46. B. Smit, T.L.M. Maesen, Nature 374 (1995) 42-44.

47. K. Mlekodaj, K. Tarach, J. Datka, K. Gora-Marek, W. Makowski, Micropor. Mesopor. Mater. 183 (2014) 54-61.

48. M. Thommes, Chem. Ing. Tech. 82 (2010) 1059-1073.

49. J. Datka, M Kawałek, K Góra-Marek, Appl. Catal. A: Gen. 243 (2003) 293-299.

50. J. Datka, K. Góra-Marek, Catal. Today 114 (2006) 205-210.

51. L. Wang, J. Zhang, X. Yi, A. Zheng, F. Deng, Ch. Chen, Y. Ji, F. Liu, X. Meng, F.-S. Xiao, ACS Catal. 5 (2015) 2727-2734.

52. A. Zheng, H. Zhang, X. Lu, S.-B. Liu, F. Deng, J. Phys. Chem. B 112 (2008) 4496-4505.

53. A. Zheng, B. Han, B. Li, S.-B. Liu, F. Deng, Chem. Commun. 48 (2012) 6936-6938.

54. A. Zheng, S.-J. Huang, W.-H. Chen, P.-H. Wu, H. Zhang, H.-K. Lee, L.-C. de Ménorval, F. Deng, S.-B. Liu, J. Phys. Chem. A 112 (2008) 7349-7356.

55. A. M. Zheng, S.-J. Huang, S.-B. Liu, F. Deng, Phys. Chem. Chem. Phys. 13 (2011) 14889-14901.

56. G. Busca, Chem. Rev. 107 (2007) 5366-5410.

57. N.S. Nesterenko, F. Thibault-Starzyk, V. Montouilliout, V.V. Yushchenko, C. Fernandez, J.P. Gilson, F. Fajula, I.I. Ivanova, Kinet. Catal. 47 (2006) 40-48.

58. F. Thibault-Starzyk, I. Stan, S. Abelló, A. Bonilla, K. Thomas, C. Fernandez, J.-P. Gilson, J. Pérez-Ramírez, J. Catal. 264 (2009) 11-14.

59. T.K. Phung, L. Proietti Hernández, A. Lagazzo, G. Busca, Appl. Catal. A: Gen. 493 (2015) 77-89.

60. J.A. Lercher, A. Jentys, A. Brait in Mol. Sieves. Ed. H.G. Karge, J.Weitkamp, Springer-Verlag 2008, vol. 6 pp. 153-212.

61. M. Bjørgen, F. Bonino, S. Kolboe, K.P. Lillerud, A. Zecchina, S. Bordiga, J. Am. Chem. Soc. 125 (2003) 15863- 15868.

62. S.H. Li, A.M. Zheng, Y.C. Sul, H.L. Zhang, L. Chen, J. Yang, C.H. Ye, F. Deng, J. Am. Chem. Soc. 129 (2007) 11161-11171.

63. S.H. Li, S.J. Huang, W.L. Shen, H.L. Zhang, H.J. Fang, A.M. Zheng, S.B. Liu, F. Deng, J. Phys. Chem. C 112 (2008) 14486-14494.

64. Y. Chu, B. Han, A. Zheng, F. Deng, J. Phys. Chem. C 116 (2012) 12687-12695

65. T.K. Phung, G. Busca, Chem. Eng. J. 272 (2015) 92-101.

66. H. Chiang, A. Bhan, J. Catal. 271 (2010) 251-261.

67. D. Däumer, M. Seifert, W. Reschetilowski, Microporous Mesoporous Mater. 219 (2016) 66-76.

68. H. Fang, A. Zheng, J. Xu, S. Li, Y. Chu, L. Chen, F. Deng, J. Phys. Chem. C 2011, 115, 7429-7439.

69. H. Yamazaki, T. Yokoi, T. Tatsumi, J.N. Kondo, Catal. Sci. Tech. 4 (2014) 4193-4195.

70. J.N. Kondo, H. Yamazaki, R. Osuga, T. Yokoi, T. Tatsumi, J. Phys. Chem. Lett. 6 (2015) 2243-2246.

71. F.L. Bleken, K. Barbera, F. Bonino, U. Olsbye, K.P. Lillerud, S. Bordiga, P. Beato, T.V.W. Janssens, S. Svelle, J. Catal. 307 (2013) 62-73.

72. U. Olsbye, S. Svelle, M. Bjørgen, P. Beato, T.V.W. Janssens, F. Joensen, S. Bordiga, K.P. Lillerud, Angew. Chem. Int.. Ed. 51 (2012) 5810-5831.

73. R. Khare, D. Millar, A. Bhan, J. Catal. 321 (2015) 23-31.

Figure captions

Figure 1 XRD patterns of studied materials.

Figure 2 (a) Low temperature N_2 isotherms and (b) BJH pore size distributions of studied materials.

Figure 3 STEM images of bulk and micro/mesoporous zeolites.

Figure 4 QE-TPDA profiles of *n*-hexane, recorded at 10°C/min.

Figure 5 QE-TPDA profiles of cyclohexane, recorded at 10°C/min.

Figure 6 IR spectra of studied materials in the region of O-H vibration.

Figure 7 Dependence between the concentration of acid sites derived from Py sorption experiments and micropore area calculated from low temperature N_2 sorption for samples obtained from *bottom up* (■) and *top down* (◆) synthesis methods.

Figure 8 IR spectra of studied materials after CO sorption at -196 ^{o}C

Figure 9 Accessibility factor values for (a) Brønsted acid sites and (b) sum of Brønsted and Lewis acid sites (AF_{dTBPy}– blue points, AF_{PN}– red points) plotted against mesopore surface area and accessibility factor values for sum of Brønsted and Lewis acid sites plotted against (c) the ratio of S_{meso}/S_{micro} from low temperature N_2 sorption and (d) the ratio of $V_{submicro}/V_{micro}$ from QE-TPDA studies

Figure 10 (a) Conversion of ethanol, (b, d, f) yields and (c, e, g) selectivities to diethyl ether, ethylene and higher hydrocarbons (C_3+) over B-ZSM-5 (■),C-ZSM-5 (●), U-ZSM-5(▲),M1-ZSM-5 (▼), M2-ZSM-5 (◆), D1-ZSM-5 (□) and D2-ZSM-5 (○) catalysts

Figure 11 Conversion [%] and TOF [10^{-4} s^{-1}] and STY [10^{-4} $g{\cdot}s^{-1}$] values obtained at reaction temperatures of 140 ^{o}C and 220 ^{o}C plotted against concentration of intrinsic acidity expressed as C_{Py} – C_{Pn} and/or against the values of accessibility factor for both Brønsted and Lewis acid sites AF_{Pn}^{B+L} for studied zeolites B-ZSM-5 (■),C-ZSM-5 (●), U-ZSM-5(▲),M1-ZSM-5 (▼), M2-ZSM-5 (◆), D1-ZSM-5 (□) and D2-ZSM-5 (○)

Figure 12 Selectivity of catalysts B-ZSM-5 (■),C-ZSM-5 (●), U-ZSM-5(▲),M1-ZSM-5 (▼), M2-ZSM-5 (◆), D1-ZSM-5 (□) and D2-ZSM-5 (○) to DEE, $C_{2=}$ and C_{3+} products in different temperatures plotted against values of accessibility factor of acid sites (B+L)

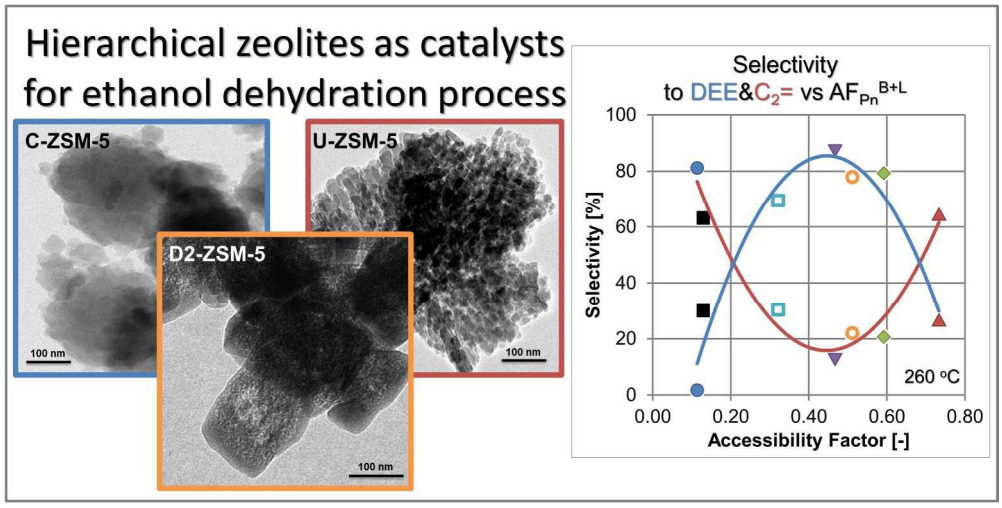

404x201mm (150 x 150 DPI)